HIGH-*Q* PHOTONIC CRYSTAL NANOBEAM CAVITY BASED ON A SILICON NITRIDE MEMBRANE INCORPORATING FABRICATION IMPERFECTIONS AND A LOW-INDEX MATERIAL LAYER

M. Grande[*], G. Calò, V. Petruzzelli, and A. D'Orazio

Dipartimento di Elettrotecnica ed Elettronica, Politecnico di Bari, Via Re David 200, Bari 70125, Italy

Abstract—We detail the optimization of a nanobeam design and show how the fabrication imperfections can affect the optical performance of the device. Then we propose the design of a novel configuration of a photonic crystal nanobeam cavity consisting of a membrane structure obtained by sandwiching a layer of Flowable Oxide (FOx) between two layers of Silicon-Nitride (SiN). Finally, we demonstrate that the presence of a low refractive index layer does not impair the performance of the nanobeam cavity that still exhibits a Q factor and mode volume V of the order of 10^5 and 0.02 $(\lambda/n)^3$, respectively.

1. INTRODUCTION

Wavelength-scale photonic crystals (PhC) have emerged as key elements for many applications ranging from cavity quantum electrodynamics [1, 2], low threshold lasers [3, 4], nonlinear optics [5–7], high performance filters [8–11], beam-splitters [12–14] and optical switches [15, 16]. In the past decade, there has been a considerable research effort to develop photonic crystal microcavities characterized by high Q-factor and small mode volume comparable to $(\lambda/n)^3$. Since light is very difficult to localize, different solutions have been proposed in literature that exploit the strong light confinement of photonic bandgaps (PBGs) in two-dimensional (2D) PBG cavities and the total internal reflection (TIR) in one dimension — the direction perpendicular to the 2D plan [17, 18] or, alternatively, the confinement of modulated one-dimensional (1D) PBGs with 2D TIR [19].

Recently, it has been theoretically and experimentally demonstrated that photonic crystal nanobeam (PhCNB) cavities based on

different material platforms can exhibit ultra high Q and small mode volume. In [20] a Silicon-Nitride (SiN) photonic crystal nanocavity with a Q factor of 1.4×10^6 and a mode volume of about 0.78 $(\lambda/n)^3$, useful for coupling to single diamond nitrogen-vacancy (NV) on a planar platform constituted by an on-chip ridge waveguide, has been designed. The fabricated nanobeam cavities [21] exhibit quality factors up to 55.000 values limited by the resolution of the grating spectrometer used for the optical characterization. In [22] the authors propose and experimentally demonstrate a deterministic method to design silicon cavities, capped with a low refractive index polymer, with $Q > 10^6$ that is strongly coupled to the feeding waveguide (on-resonance transmission $T > 90\%$). The coupling between two PhCNB cavities on a SOI substrate [23] has been exploited to demonstrate reconfigurable optical filters, operating at 1550 nm, that can be dynamically and reversibly tuned over a 9.5 nm wavelength range, by applying a potential difference directly across the nanobeams that induces an attractive electrostatic force between the two membranes. Recently, a nanocavity based on a triangular cross-section has been proposed in [24]. This new configuration allows vertical confinement and better signal collection efficiency than that of slab-based nanocavities.

The aim of this paper is to shed light on the performance of a nanobeam incorporating a FOx layer that serves as hosting material for CdSe/CdS core/shell nanocrystals in the quantum dot emission wavelength range of our interest 575–595 nm. FOx is a flowable oxide than can be successfully doped with nanocrystals and can spin coated on flat surface and thermally treated in order to get solid layers. In a previous paper [25] a similar technology has been optimized for 2D Photonic Crystal cavities. In order to assess the performance of the nanobeam, in this paper we start with the optimization of the Q factor and then, by introducing fabrication imperfections compatible with the technological process, we demonstrate that a pseudo-casual disorder introduced in the taper region holes located in proximity of the nanocavity can cause a detrimental decreasing of the performances while it does not alter the nanobeam performance if placed in the mirror region. Subsequently a novel configuration of a PhCNB cavity consisting of a membrane structure obtained by sandwiching a layer of Flowable Oxide (FOx) between two layers of Silicon-Nitride is presented. We demonstrate that the presence of the low refractive index layer does not affect the performance of the nanobeam cavity that exhibits a Q factor of the order of 10^5 and small mode volume of the order of about 0.02 $(\lambda/n)^3$. The low index layer can be exploited to host CdSe/CdS core/shell nano-emitters leading to a new class of active optical devices [25] where the colloidal nano-crystals can be

chemically sensitized and deposited by spin-coating or drop-casting. These structures could be used as active material and high Q factor could lead to the realization of integrated sources for devices devoted to sensing applications.

2. NANOBEAM CAVITY DESIGN

Firstly, we analyzed PhCNB cavities proposed formed by a Silicon Nitride membrane suspended in air. Figure 1(a) shows the layout of the 1D photonic crystal nanobeam cavity while Figure 1(b) illustrates the refractive index profile along the y-axis and shows that the SiN thickness h is equal to 200 nm.

    In the following numerical analysis, the dispersion of the SiN has not been taken into account since it can be considered constant in the range of our interest that is only tens of nanometers wide as shown subsequently. Therefore the refractive index of the SiN, n_{SiN} has been fixed equal to 2.

    The engineering process has been based on the optimization of the cavity length. The membrane width w has been fixed equal to 300 nm. The photonic crystal mirrors have been realized by means of 17 circular holes. The hole spacing p and the hole radius r have been fixed in order to centre the resonances in the range of wavelengths where chemically synthesized nanocrystals (NCs), such as CdSe/CdS core/shell nanocrystals, exhibit emission peaks [25]. The tapered regions are symmetrically located with respect to the nanocavity and each taper is constituted by 7 holes. The tapered regions have been designed in order to minimize the modal mismatch between the wire monomode and the PhC mirror Bloch mode [26] that show different effective refractive indexes. Therefore the taper allows an adiabatic transition between these two modes obtaining, as a result, the decreasing of the scattering losses. The nanocavity is localized between two mirror/taper sections and L_c defines the cavity length (Figure 1(a)).

    The numerical analysis of these structures has been performed by a three-dimensional Finite Difference Time Domain (FDTD) code [27]. Since the nanobeam is completely symmetric with respect to the origin, the computational domain has been reduced by a factor equal to 1/8 and even symmetry conditions for the E_z component of the electric field has been added along the three axes at $x = 0\,\mu\mathrm{m}$, $y = 0\,\mu\mathrm{m}$ and $z = 0\,\mu\mathrm{m}$, respectively. Moreover the computational domain has been bounded by perfectly matched layers (PMLs) on top and on the sides of the nanobeam surrounded by air. The computational mesh has a grid step of $p/16$ along each axis to capture the effects of field
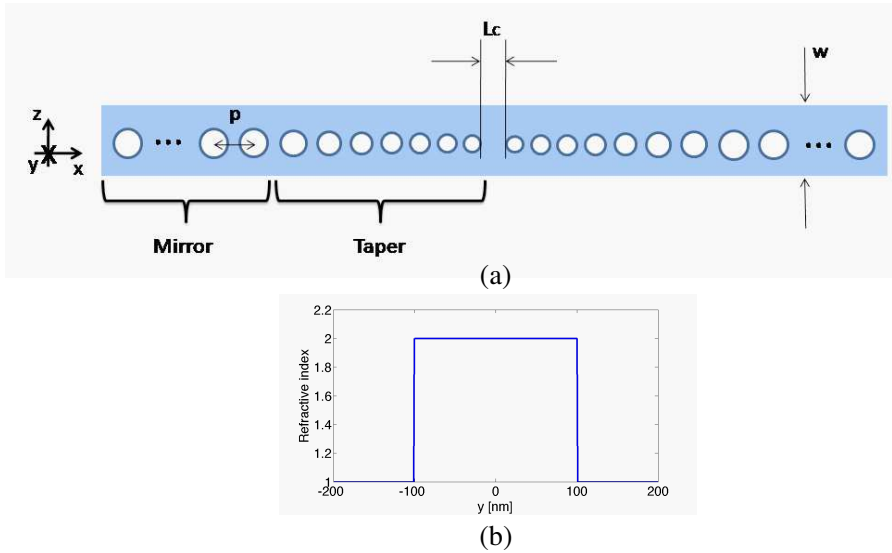
(a)

(b)

Figure 1. (a) Sketch of the photonic crystal nanobeam cavity. (b) Refractive index profile along the y-axis in absence of the FOx layer with $h = 200\,\mathrm{nm}$.

penetration on the dielectric regions. It is worth pointing out that this spatial resolution is adequate for the determination of the Q factor since a grid step of $p/16$ and $p/24$ along each axes leads to the same results. The source field has the following components E_x, H_y, E_z and the wave rises from a total field/scattered field (TF/SF) section placed in the middle of the cavity in a random low-symmetry position (e.g., $x = 0.026\,\mu\mathrm{m}$, $y = 0.05\,\mu\mathrm{m}$ and $z = 0.01\,\mu\mathrm{m}$) in order to facilitate the computing of the Q factor as shown hereinafter. The input wave has a sinusoidal time dependence, whose free-space wavelength is centred at $585\,\mathrm{nm}$, and it is modulated by a Gaussian signal. Finally a time monitor for the evaluation of the spectral response and Q factor has been placed in the cavity: also in this case, the position has been chosen in order to avoid symmetric position.

We estimate the resonant wavelength and the cavity Q factor, defined as $Q = \omega_0 \tau$ where $\tau = $ *(stored energy/power lost)* is the characteristic decay time in the cavity, by means of an Advanced Harmonic Analysis based on the Padè interpolation of the Discrete Fourier Transform (DFT) of the computed mode profile for both **E** and **H** field components [27]. Moreover we evaluate the conventional mode volume V given by the ratio of the total electric field energy to the maximum of the electric field energy density [27].

We start our analysis by locating the nanobeam resonance wavelength in the quantum dot emission range of our interest (575–595 nm) [25, 28], adopting a geometrical configuration characterized by the following parameters: hole spacing $p = 222$ nm, hole radius $r = 70$ nm, tapering region constituted by 7 holes with a linear increase of the hole radius in the range 55–70 nm and of the hole spacing in the range 190–222 nm, respectively. Table 1 reports the simulation results when the cavity length L_c is varied in the range from 65 nm to 92 nm. As we can infer from these data the optimum evaluated Q-factor is equal to 855270, while the mode volume V is equal to 0.016 $(\lambda/n)^3$ for a cavity length $L_c = 77$ nm. It is worth stressing that when L_c is varied, the resonant wavelength Λ experiences a slight red-shift but falls always within the range of our interest. Moreover Table 1 reports also the Purcell factor, $F_p = 3/(4\pi^2)(\lambda/n)^3 Q/V$, showing that the maximum value occurs at the maximum value of the Q factor. It is worth noting that this behavior is valid for all the nanobeams that will be presented hereinafter therefore the following analysis will be only related to the Q factor examination.

Figure 2 shows the plot of the Q factor and the mode volume when the cavity L_c is varied confirming that the better result has been obtained for the PhCNB cavity resonating at 581 nm. Moreover the plot illustrates that the Q-factor curve assumes a bell-shaped curve

Table 1. Q-factor, mode volume V, resonant wavelength Λ and Purcell factor for the nanobeam structure characterized by a total membrane height $h = 200$ nm, in absence of the FOx layer, as a function of the cavity length L_c.

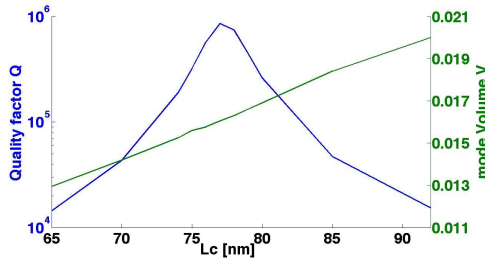| L_c [nm]	Q	V $(\lambda/n)^3$	Λ [µm]	F_p
65	14368	0.01294	0.57636-	84376
70	43341	0.0142	0.57863	231938
74	188660	0.01524	0.58032	940711
75	321060	0.0156	0.58072	1563950
76	571840	0.01577	0.58112	2755524
77	855270	0.01605	0.58150	4049391
78	742530	0.01633	0.58188	3455328
79	445200	0.01662	0.58226	2035568
80	260980	0.01692	0.58262	1172110
85	47087	0.01849	0.58436	193519
92	15347	0.02004	0.58660	58195

Figure 2. Quality factor as a function of the nanocavity length L_c for the free-standing PhC characterized by the following parameters: hole spacing $p = 222$ nm and hole radius $r = 70$ nm.

with a relative maximum point at the optimum cavity length typical of this type of PhCNB [29] while the mode volume V varies linearly in the range 0.013–0.020 $(\lambda/n)^3$.

3. EFFECT OF THE FABRICATION IMPERFECTIONS

The proposed device can be fabricated, following a similar technological protocol reported in [25], by means of six main steps a)–f): a) an initial SiN layer could be deposited by means of Plasma Enhanced Chemical Deposition on a Silicon substrate and subsequently b) a FOx layer, containing the active material, could be spin coated. At this stage the FOx layer could be thermally treated in order to get a solid layer. Subsequently c) a second layer of SiN could be deposited with the same technological step. The layout, defined by the geometrical parameters, could be transferred by means of d) an Electron Beam Lithography (EBL) step to a positive electronic resist that can be employed as a mask for the following e) etching process. Finally the membrane could be released by f) removing the Silicon substrate in a KOH-based solution bath. This fabrication protocol can introduce fabrication imperfection due to the disorder that can be related to the spatial position and the size of the PhC holes, respectively. The former is related to the stability of the electron beam while the latter is mainly related to the area dose during the exposure step, respectively. In this paragraph the effect of the fabrication imperfection will be analyzed. In particular, the nanobeam cavity characterized by hole spacing $p = 222$ nm, hole radius $r = 70$ nm, $L_c = 77$ nm, has been considered to verify how much the fabrication imperfections can influence the structure performances. The analysis has been performed by introducing some disorder in the structure, i.e., pseudo-casual

Table 2. Q factor and mode volume V as a function of the disorder introduced on the hole spacing p.

Disorder Position	Error offset	Q	V $(\lambda/n)^3$
Mirror	$[-2\ -1\ 0\ 1\ 1\ 2\ -1\ -2$ $2\ 0\ 1\ -1\ 0\ 2\ -1\ -2\ 1]$	743587	0.01607
Taper	$[\mathbf{0}\ -2\ 1\ 1\ -1\ 2\ 0]$	93045	0.01577
	$[\mathbf{0}\ 1\ -1\ -2\ 1\ 0\ 2]$	95190	0.01608
	$[\mathbf{0\ 0}\ -1\ 1\ 2\ 0\ -2]$	129110	0.01601
	$[\mathbf{0\ 0\ 0}\ -1\ 1\ 2\ -2]$	183140	0.01602
Taper + Mirror	$[0\ 1\ -1\ -2\ 1\ 0\ 2\ -2$ $-1\ 0\ 1\ 1\ 2\ -1\ -2\ 2$ $0\ 1\ -1\ 0\ 2\ -1\ -2\ 1]$	65729	0.0161

changes of the hole spacing p and of the hole radius r. The error sequences have been generated by introducing new variables, namely Sx and Rx, which define, respectively, the change of the hole spacing $\Delta p = p_{\text{unmodified}} - p_{\text{disorder}}$, i.e., the shift (towards the right or the left along the x-axis, as a function of the sign of Sx) of the hole centre with respect to the original location, and the change of the hole radius $\Delta r = r_{\text{unmodified}} - r_{\text{disorder}}$.

Table 2 reports the evaluated Q factor and mode volume V as a function of the disorder introduced on the hole spacing p when different sequences of Sx are considered. In particular the table resumes the results obtained for the sequences Sx where the Δp is varied in the range $(-2\,\text{nm},\ -1\,\text{nm},\ 0\,\text{nm},\ +1\,\text{nm},\ +2\,\text{nm})$. The disorder is introduced only in the mirror regions or in the taper regions and finally in both regions. Finally the order of the error offset follows the position of the hole in the mirror and taper regions, respectively. It is worth stressing that these values have been adopted because they refer to the error introduced by a standard electron beam lithography process.

As can be infered, the disorder introduced in the mirror does not alter the performance of the structure. On the contrary there is a dramatic decrease of the Q factor when the disorder is introduced in the taper region, also in the case of little changes of the hole spacing, since the matching condition is lost. Moreover the Q factor decreasing is more evident when the disorder affects the holes located in proximity of the cavity. In order to emphasis this trend, the zeros closer to the nanocavity have been highlighted in bold in Table 2.

Table 3 reports the evaluated Q factor and mode volume V as a function of the disorder introduced on the hole radius r when different sequences of Rx are considered. In particular the table

Table 3. Q factor and mode volume V as a function of the disorder introduced on the hole radius r for $Rx = 5$ nm (italic) and $Rx = 2$ nm (normal), respectively.

Disorder Position	Error offset	Q	V $(\lambda/n)^3$
Taper	$[0\ 2\ -2\ -5\ 0\ 0\ 5]$	*21752*	*0.01604*
	$[0\ 0\ -5\ 2\ 5\ 0\ -2]$	*17696*	*0.01641*
	$[0\ 1\ -1\ -2\ 0\ 0\ 2]$	94192	0.01602
	$[0\ 0\ -2\ 1\ 2\ 0\ -1]$	92689	0.01618
	$[0\ 0\ 0\ 1\ -2\ -1\ 2]$	151456	0.01602

resumes the results obtained for the sequences $R_x = 2$ nm $[\Delta r = (-2, -1, 0, +1, +2)]$ and $R_x = 5$ nm $[\Delta r = (-5, -2, 0, +2, +5)]$ when the disorder is introduced in the taper regions. Also in this case, the Q factor decreasing is more consistent when the disorder affects the holes located in proximity of the cavity.

4. TECHNOLOGICAL OPTIMIZATION AND FOx INTRODUCTION

Even if the nanobeam cavity, previously analysed and characterized by hole spacing $p = 222$ nm, hole radius $r = 70$ nm and $L_c = 77$ nm, shows a high quality factor, the geometrical parameters limit the effective realization of the device since a) the cavity length is very short, b) the Q factor varies very rapidly when the L_c is changed and c) the minimum distance between the edge of two adjacent holes is only about 82 nm. It is worth pointing out that a very high aspect ratio is desired when dealing with PhC holes and hence the hole vertical sidewalls must be very vertical. In the technology process optimization it can be found that usually V-shaped holes or holes that are enlarged in the middle can be obtained. Consequently a larger distance between two adjacent holes can facilitate the fabrication process and avoid the membrane collapse. Therefore the device has been optimized varying simultaneously the period and the radius in the following procedure: firstly the radius has been modified in order to keep the difference between the two outer holes constant and equal to 15 nm; subsequently the period has been changed in order to place the resonant wavelength of the nanobeam in the quantum dot emission wavelength range of our interest (575–595 nm).

Following these procedures, two different nanobeams have been optimised: A) $p = 218$ nm, $r = 65$ nm, and B) $p = 215$ nm, $r = 60$ nm,
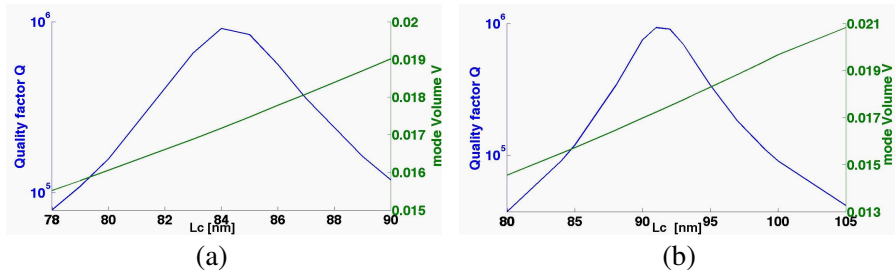
Figure 3. Quality factor as a function of the nanocavity length for the free-standing PhC characterized by the following parameters: (a) nanobeam A: $p = 218\,\text{nm}$, $r = 65\,\text{nm}$, and (b) nanobeam B: $p = 215\,\text{nm}$, $r = 60\,\text{nm}$, respectively.

respectively.

Figure 3 proves that the two configurations reach a Q factor of $9.1482\ 10^5$ and $9.2984\ 10^5$ for the nanobeams A and B, respectively.

The comparison of the plots shown in Figures 3(a), 3(b) reveals that the best candidate is the nanobeam B since 1) the high Q factor values ($+10\%$) are reported in the range 85–100 nm, 2) $L_c = 91\,\text{nm}$ ($+24\%$) and 3) the minimum distance between two adjacent holes is equal to 95 nm ($+16\%$).

Starting from this optimized design, the effect of the introduction of the FOx layer on the nanobeam B performance has been analysed. In order to resolve adequately the presence of the FOx layer, the grid step of $p/48$ along the y-axis has been adopted. Figure 4(a) shows the new refractive index profile in y-axis direction while the arrangement and the position of the holes in the xz-plane is the same as in the sketch reported in Figure 1(a). The nanobeam is obtained by sandwiching a layer of FOx (refractive index, n_{FOx} is equal to 1.4) between two layers of Silicon Nitride.

Figure 4(b) shows the linear behaviour of the Q factor when the FOx layer thickness t is varied in the range 0 nm to 60 nm with a step of 10 nm. As one can infer from the plot inspection, the introduction of the FOx layer does not deteriorate the nanobeam performance since the Q factor value is still high. Moreover Figure 4(c) also demonstrates that the nanocavity resonant wavelength experiences a shift toward lower wavelength while the mode volume rises when the FOx layer thickness is increased. These results show that a nanobeam with FOx layer thickness of 10 nm shows a Q factor, a mode volume V, and a resonant wavelength equal to $8.7\ 10^5$ (only 6% less), 0.01775 and 577 nm, respectively. Therefore the nanobeam consisting of a low

(a)

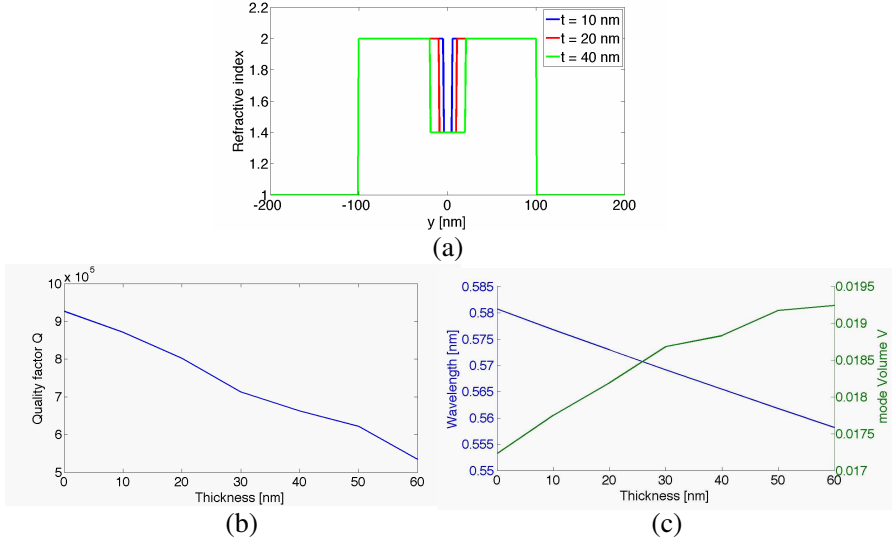(b)   (c)

Figure 4. (a) Refractive index profile along the y-axis for a 10 nm-thick, 20 nm-thick and 40 nm-thick FOx layer, respectively; (b) Quality factor vs FOx layer thickness for the configuration of nanobeam B; (c) Quality factor and mode volume as a function of the FOx layer thickness.

refractive index layer sandwiched between two SiN layers is still able to realize a very high Q factor nanocavity and revealing high performance comparable (even better if the mode volume is considered) with the nanobeam B previously reported.

5. CONCLUSION

In this paper, the effect of the fabrication imperfections, compatible with the technological process, on the performances of a nanobeam PhC cavity has been discussed. We demonstrate that a pseudo-casual disorder introduced in the taper region holes located in proximity of the nanocavity can cause a detrimental decreasing of the performances while it has a smaller impact if localized in the mirror region. These findings are in agreement with the experimental results reported in literature where designed Q factor of the order of 10^6 falls down to value of the order of 10^4–10^5 when real devices are considered. Finally, we propose the design of a novel configuration of a photonic crystal nanobeam cavity consisting of a membrane structure obtained

by sandwiching a layer of Flowable Oxide between two layers of Silicon-Nitride. We demonstrate that the presence of the low refractive index layer does not affect the performance of the nanobeam cavity that exhibits a Q factor of the order of 10^5 and a small mode volume of about 0.017–0.019 $(\lambda/n)^3$ in the range of our interest. These results show how the technology protocol developed in previous works [25, 28] can be applied to the realization of nanobeams that exhibit Q factor of the order of 10^5–10^6 and a small mode volume with FOx layer thicknesses consistent with technological process such as spin-coating (about few nanometers).

These outcomes pave the way for new devices where nano-emitters such as nano-crystals and quantum dots can be integrated in passive structures for different applications ranging from QED, new optical sources up to active devices with simple and very controllable fabrication processes.

ACKNOWLEDGMENT

REFERENCES

1. Englund, E., A. Faraon, I. Fushman, N. Stoltz, P. Petroff, and J. Vucković, "Controlling cavity reflectivity with a single quantum dot," *Nature*, Vol. 450, No. 7171, 857–861, 2007.

2. Hennessy, K., A. Badolato, M. Winger, D. Gerace, M. Atatüre, S. Gulde, S. Fält, E. L. Hu, and A. Imamoğlu, "Quantum nature of a strongly coupled single quantum dot-cavity system," *Nature*, Vol. 445, No. 7130, 896–899, 2007.

3. Paintier, O., R. K. Lee, A. Scherer, A. Yariv, J. D. O'Brien, P. D. Dapkus, and I. Kim, "Two-dimensional photonic band-gap defect mode laser," *Science*, Vol. 284, 1819–1821, 1999.

4. Loncar, M., T. Yoshie, A. Scherer, P. Gogna, and Y. M. Qiu, "Low-threshold photonic crystal laser," *Appl. Phys. Lett.*, Vol. 81, 2680–2682, 2002.

5. Antonucci, D., D. De Ceglia, A. D'Orazio, M. De Sario, V. Marrocco, V. Petruzzelli, and F. Prudenzano, "Enhancement of SHG efficiency in doubly resonant 2D-photonic crystal

microcavity," *Optical and Quantum Electronics*, Vol. 39, Nos. 4–6, 353–360, 2007.

6. McCutcheon, M. W., J. F. Young, G. W. Rieger, D. Dalacu, S. Frederick, P. J. Poole, and R. L. Williams, "Experimental demonstration of second order processes in photonic crystal microcavities at submilliwatt exitation powers," *Physics Review B*, Vol. 76, 245104, 2007.

7. Antonucci, D., A. D'Orazio, D. De Ceglia, M. De Sario, V. Marrocco, V. Petruzzelli, and F. Prudenzano, "A doubly resonant photonic crystal microcavity for second harmonic generation," *Fiber and Integrated Optics*, Vol. 26, No. 5, 271–288, 2007.

8. D'Orazio, A., M. De Sario, V. Marrocco, V. Patruzzelli, and F. Prudenzano, "Photonic crystal drop filter exploiting resonant cavity configuration," *IEEE Transactions on Nanotechnology*, Vol. 7, No. 1, 10–13, 2008.

9. Banai, H. A. and A. Rostami, "A novel proposal for passive all-optical demultiplexer for DWDM systems using 2-D photonic crystals," *Journal of Electromagnetic Waves and Applications*, Vol. 22, No. 4, 471–482, 2008.

10. Grande, M., L. O'Faolain, T. P. White, M. Spurny, A. D'Orazio, and T. Krauss, "Optical filter with very large stopband ($\approx$ 300 nm) based on a photonic crystal vertical directional coupler," *Optics Letters*, Vol. 34, No. 21, 3292–3294, 2009.

11. Stomeo, T., M. Grande, G. Rainò, A. Passaseo, A. D'Orazio, R. Cingolani, A. Locatelli, D. Modotto, C. De Angelis, and M. De Vittorio, "Optical filter based on two coupled PhC GaAs-membranes," *Optics Letters*, Vol. 35, No. 3, 411–413, 2010.

12. Awasthi, S. K. and S. P. Ojha, "Wide-angle broadband plate polarizer with 1D photonic crystal," *Progress In Electromagnetics Research*, Vol. 88, 321–335, 2008.

13. Li, Y., P. Gu, M. Li, H. Yan, and X. liu, "Research on the wide-angle and broadband 2D photonic crystal polarization splitter," *Journal of Electromagnetic Waves and Applications*, Vol. 20, No. 2, 265–273, 2006.

14. Shi, Y., "A compact polarization beam splitter based on a multimode photonic crystal waveguide with an internal photonic crystal section," *Progress In Electromagnetics Research*, Vol. 103, 393–401, 2010.

15. Maleki Javan, A. R. and N. Granpayeh, "Fast Terahertz wave switch/modulator based on photonic crystal structures," *Journal of Electromagnetic Waves and Applications*, Vol. 23, Nos. 2–3,

203–212, 2009.

16. Calò, G., A. D'Orazio, M. Grande, V. Marrocco, and V. Petruzzelli, "Active InGaAsP/InP photonic bandgap waveguides for wavelength-selective switching," *IEEE Journal of Quantum Electronics*, Vol. 47, No. 2, 172–181, Feb. 2011.

17. Song, B. S., S. Noda, T. Asano, and Y. Akahane, "Ultra-high-Q photonic double-heterostructure nanocavity," *Nature Materials*, Vol. 4, No. 3, 207–210, 2005.

18. Kuramochi, E., M. Notomi, M. Mitsugi, A. Shinya, and T. Tanabe, "Ultrahigh-Q photonic rystal nanocavities realized by the local width modulation of a line defect," *Appl. Phys. Lett.*, Vol. 88, 041112, 2006.

19. Notomi, M., E. Kuramochi, and H. Taniyama, "Ultrahigh-Q nanocavity with 1D photonic gap," *Optics Express*, Vol. 16, No. 15, 11095–11102, 2008.

20. Md Zain, A. R., N. P. Johnson, M. Sorel, and R. M. De la Rue, "Ultra high quality factor one dimensional photonic crystal/photonic wire micro-cavities in silicon-on-insulator (SOI)," *Optics Express*, Vol. 16, No. 16, 12084–12089, 2008.

21. Khan, M., T. Babinec, M. W. McCutcheon, P. Deotare, and M. Loncar, "Fabrication and characterization of high-quality factor silicon nitride nanobeam cavities," *Optics Letters*, Vol. 36, No. 3, 421–423, 2011.

22. Quan, Q., P. B. Deotare, and M. Lonkar, "Photonic crystal nanobeam cavity strongly coupled to the feeding waveguide," *Appl. Phys. Lett.*, Vol. 96, 203102, 2010.

23. Frank, I. W., P. B. Deotare, M. W. McCutcheon, and M. Loncar, "Programmable photonic crystal nanobeam cavities," *Optics Express*, Vol. 18, No. 8, 8705–8712, 2010.

24. Bayn, I., B. Meyler, J. Salzman, and R. Kalish, "Triangular nanobeam photonic cavities in single-crystal diamond," *New Journal of Physics*, Vol. 13, 025018, 2011.

25. Qualtieri, A., F. Pisanello, M. Grande, T. Stomeo, L. Martiradonna, G. Epifani, A. Fiore, A. Passaseo, and M. De Vittorio, "Emission control of colloidal nanocrystals embedded in Si_3N_4 photonic crystal H_1 nanocavities," *Microelectronic Engineering*, Vol. 87, 1435–1438, 2010.

26. Lalanne, P., C. Sauvan, and J. Hugonin, "Photon confinement in photonic crystal nanocavities," *Laser & Photonics Reviews*, Vol. 2, 514–526, 2008.

27. RSoft Suite, FullWAVE user guide.

28. Pisanello, F., L. Martiradonna, A. Qualtieri, T. Stomeo, M. Grande, P. P. Pompa, R. Cingolani, A. Bramati, and M. De Vittorio, "Silicon nitride PhC nanocavities as versatile platform for visible spectral range devices," *Photonics and Nanostructures — Fundamentals and Applications*, Aug. 22, 2011, ISSN 1569-4410, Available online, 10.1016/j.photonics.2011.08.003.

29. Rivoire, K., S. Buckley, and J. Vučković, "Multiply resonant high quality photonic crystal nanocavities," *Appl. Phys. Lett.*, Vol. 99, 013114, 2011.